Ethylene removal by Ag-based ZSM-5 adsorbents for the preservation of climacteric fruits.

R. Ferreira[a], H. Lopes[a], J.P. Lourenço[a,b], J.M. Silva[a,c], I.M. João[c,d], M. F. Ribeiro[a], A. Fernandes[a*]

[a]*Centro de Química Estrutural, Institute of Molecular Sciences, Instituto Superior Técnico, Universidade de Lisboa, Av. Rovisco Pais, 1049-001, Lisboa, Portugal,* [b]*Faculdade de Ciências e Tecnologia, Universidade do Algarve, Campus de Gambelas, 8005-139 Faro, Portugal,* [c]*Instituto Superior de Engenharia de Lisboa, IPL, R. Conselheiro Emídio Navarro, 1959-007, Lisboa, Portugal,* [d]*CEG-IST, Instituto Superior Técnico, Universidade de Lisboa, Av. Rovisco Pais, 1049-001 Lisboa, Portugal.*

*corresponding authors: Auguste Fernandes, auguste.fernandes@tecnico.ulisboa.pt, Centro de Química Estrutural (CQE), 1 Avenida Rovisco Pais, 1049-001 Lisboa (Portugal)

Abstract:

Ethylene removal is crucial for fruits and vegetables preservation because even a very low concentration (<0.1ppm) can induce ripening during storage and transportation. Ag^+ exchanged ZSM-5 zeolites were investigated as adsorbents for the efficient removal of ethylene. Two ZSM-5 materials (Si/Al ratios of 15 and 40), with different amounts of Ag (up to 6 % by weight) and two compensating cations, Na^+ and H^+, were used for this purpose. The adsorbents were characterized by X-ray Diffraction, diffuse reflectance spectroscopy and H_2-TPR experiments. Their performance in ethylene adsorption was determined by the means of breakthrough curves experiments, mimicking the atmospheric conditions of industrial fruits cold storage chambers, particularly the high relative humidity levels. Results show that adsorbents are highly efficient in removing ethylene (max. 500 $\mu mol.g^{-1}$ in the absence of water). Monovalent Ag^+ species have been identified as the main contributors to the excellent performance of the different adsorbents, as they can easily interact with ethylene through strong π interaction. Moreover, statistical analysis (ANOVA) results confirmed that, in the presence of water, Ag-based ZSM-5 materials with a higher Si/Al ratio and Na^+ as the charge balancing cation, i.e., those with a higher hydrophobic character, are the best adsorbents for ethylene removal.

Keywords: Ethylene; exchanged Ag^+; fruit preservation; breakthrough curves; competitive adsorption.

1. Introduction

Today, food waste is one of the major concerns for the agrifood industry, with millions of tons wasted globally every year. Fruits and vegetables are no exception, as almost half of their annual production is lost along the distribution supply chain, above all, after harvest and before consumption steps. Climacteric fruits, in particular, suffer from continuous post-harvesting ripening because of ethylene, a natural hormone that induces ripening process and is continuously released by fruits, even at very low concentration levels of ethylene exposure [1]. Therefore, the control and removal of ethylene during fruit transportation and storage are top priorities to significantly reduce waste in fruits and vegetables.

Many pathways have been used to address the ethylene problem [1]. Utilization of chemical inhibitors is a solution that has been applied by most of the fruits companies. Currently, 1-methylcyclopropene (1-MCP) is the most widely adopted compound. This inhibitor binds to fruit receptors, blocking the ethylene production and, thus, preventing the ripening process [2]. However, some drawbacks may arise from the use of 1-MCP as the effect of this chemical inhibitor on fruits physiological disorder is still not fully understood. Also, chemical treatment of vegetables and fruits generally faces a strong public resistance. Another pathway is the use of controlled cold storage chambers. In this case, the atmosphere within the chambers can be controlled (in very different ways) to preserve the freshness of fruits, while preventing ripening. Nowadays, modern dynamic cold storage chambers are equipped for the control of several critical parameters, such as low storage temperature, high relative humidity, CO_2, O_2, C_2H_4, among others. This sophisticated control allows to slow down fruit respiration and minimize ethylene production, extending the shelf-life of the final products [3].

However, ethylene production is still an important issue, given that even traces of ethylene (concentrations as low as 0.1 ppm) can have a significant impact on fruit preservation, even in cold storage chambers with controlled atmospheres. Several methods can be employed to decrease ethylene concentrations, e.g., chemical oxidation ($KMnO_4$), adsorption (using activated carbons, zeolites), and advanced oxidation systems (such as ozone, thermal/catalytic, photocatalysis, etc.) [1,2]. Ethylene adsorption using an inexpensive and highly porous adsorbent can be a promising alternative. This process is simple, cost-effective, and sustainable, provided that the adsorbent used demonstrates a high ethylene adsorption capacity and can be efficiently reused [2]. Zeolites are strong potential candidates for ethylene adsorption, as they present many advantages over other supports like clays and activated

carbons. They are highly crystalline aluminosilicates, they possess high surface areas, substantial pores volumes, and also negative charges balanced by compensating cations. Moreover, zeolites are commercially available and easily regenerable. They can be used in their original form or as a support for metals, metal oxides, or cationic species (clusters, nanoparticles, framework or charge-balancing cations, etc.) [4]. Metals inside zeolites pores can be beneficial since they readily interact with ethylene, by the so-called π interaction [5]. Noble metals like Pd have been shown to strongly interact with C_2H_4, significantly enhancing the ethylene adsorption capacity of the adsorbents [6,7]. However, due to their high cost, cheaper solutions have been explored, including metal-exchanged zeolites, natural zeolites, zeolites exchanged with alkaline elements (Na^+, K^+, etc.) [8–12] and metal cations-exchanged zeolites. In particular, Ag-based zeolite materials have been extensively studied, given that monovalent Ag^+ species are prone to such strong π interaction with ethylene molecules [13–17]. Moreover, most of the literature reports focus on ethylene adsorption experiments conducted under dry conditions, i.e., in the absence of water. However, in industrial cold storage fruit chambers, the water content can vary a lot (50-100 % relative humidity RH), to maintain quality of fruits and vegetables under storage [18]. Therefore, studies on ethylene adsorption should ideally compare adsorption experiments under both wet and dry conditions. Interestingly, theoretical studies by Horvatits *et al.* [19,20] have revealed that Ag^+ ion-exchanged species, along with Ag_2O species, could interact with ethylene molecules via π interaction, but not protonic H^+ species (Brönsted acid sites). In the particular case of ethylene/water co-adsorption in Ag^+ ion-exchanged SSZ-13 zeolite [20], the authors concluded that Ag^+ adsorption sites could easily host two adsorbed molecules, such as two ethylene molecules, two water molecules or one ethylene + one water molecules. This interesting result shows that water can readily compete with ethylene for the adsorption sites, as already observed by Kang *et al.* [21] and Lee *et al.* [22] who investigated Ag-based zeolites (BEA and ZSM-5, respectively) for hydrocarbons trapping (including ethylene) under cold-start conditions.

In this work, we studied the ethylene adsorption capacity of Ag-based ZSM-5 zeolites, both in the presence and absence of water. Ag-based ZSM-5 adsorbents were prepared with different silver concentrations, by using commercially available ZSM-5 materials with two different Si/Al ratio and two different starting compensation cations (Na^+ and H^+). The introduction of silver was performed by ion exchange. The maximum ethylene adsorption capacity was

evaluated by the means of breakthrough curves (BC) experiments under both dry and wet conditions. A statistical analysis, employing a model based on analysis of variance (ANOVA), was performed in order to understand the relationship between ethylene adsorption capacity and adsorbents parameters (Si/Al ratio, Ag amount, etc.). Finally, various characterization methods were applied to elucidate the nature of the different Ag species present onto the adsorbents and to determine their role on the ethylene adsorption behavior.

2. Experimental section

2.1. Materials and reagents

Commercial NH_4ZSM-5 zeolites, i.e., CBV3024E, CBV5524G and CBV8014 (with the respective Si/Al ratios of 15, 25 and 40) were purchased from Zeolyst company. Silver nitrate (> 99 %) and sodium nitrate (99 %) were both obtained from Sigma-Aldrich.

2.2. Preparation of Na-ZSM-5 material

NH_4ZSM-5 zeolites (Si/Al= 15 and 40) were used to prepare NaZSM-5 materials by ion exchanging parent NH_4-forms with a $NaNO_3$ solution. In a typical run, 2.5 g of NH_4ZSM-5 powder (Si/Al of 15 or 40) is suspended in a 250 ml aqueous solution of a sodium nitrate (1 M) and the following mixture is stirred for 1 hour at room temperature (RT). Afterward, the sample was recovered by filtration, washed thoroughly with distilled water and dried in an oven at 80 ºC overnight. The ionic exchange was repeated twice to ensure a complete NH_4^+ cations exchange by Na^+ ones.

2.3. Preparation of Ag-based ZSM-5 adsorbents

Ag-based ZSM-5 adsorbents were prepared by using both NH_4ZSM-5 and NaZSM-5 starting materials. The procedure consisted in introducing Ag through ion exchange (IE), where 2.5 g of zeolite was suspended in 250 ml of an aqueous solution of silver nitrate ($AgNO_3$). The mixture was stirred for 24 hours at RT in the dark. Afterward, the adsorbent materials were recovered by filtration, washed thoroughly with distilled water and finally dried in an oven at 80 ºC overnight. Two different concentrations, 0.003 and 0.01 M, were used and the ion exchanges were carried out 1, 2 or 3 times, depending on the desired amount of Ag. The

resulting adsorbent materials were calcined at 500 ºC under air flow (4 $L.h^{-1}.g^{-1}$) for 6 hours. The zeolites were then named as follows: xAg-Y(z), where x is the amount of Ag, Y is the compensating cation and z is the Si/Al ratio. For comparison purposes, the 6.1Ag-H(40) sample (Si/Al = 40, H^+ compensating cation) was prepared using the incipient wetness impregnation (IWI) method, to achieve a final Ag content of about 6 % by weight. All the adsorbents were finally calcined at 500 ºC under air for 6 h. Table 1 provides details on the different Ag-based ZSM-5 adsorbents prepared, the experimental conditions for ion exchange and the final Ag amounts reached. After Ag introduction and subsequent calcination, the two compensating cations (in addition to Ag) are either Na^+ or H^+ (resulting from NH_4^+ decomposition), depending on the starting ZSM-5 material used.

Table 1. Ion exchange conditions for Ag-based adsorbents preparation ($AgNO_3$ aq. solution, RT, under dark, 24 h).

Sample	**cation**	**Si/Al**	**Metal introduction protocol[a]**		**Ag content (wt. %)[b]**
0.7Ag-H(15)	H^+	15	0.003 M	1x	0.7
3.1Ag-H(15)	H^+	15	0.01 M	1x	3.1
4.3Ag-Na(15)	H^+	15	0.01 M	1x	4.3
4.6Ag-H(15)	Na^+	15	0.01 M	3x	4.6
6.1Ag-Na(15)	H^+	15	0.01 M	3x	6.1
2.2Ag-H(25)	H^+	25	0.01 M	1x	2.2
3.4Ag-H(25)	H^+	25	0.01 M	2x	3.4
0.5Ag-H(40)	H^+	40	0.003M	1x	0.5
1.9Ag-H(40)	H^+	40	0.01M	1x	1.9
3.2Ag-Na(40)	Na^+	40	0.01M	1x	3.2
2.8Ag-H(40)	H^+	40	0.01M	3x	2.8
3.9Ag-Na(40)	Na^+	40	0.01M	3x	3.9
6.1Ag-H(40)[c]	H^+	40		IWI	6.1

[a]salt solution concentration and number of IEs; [b]from chemical analysis; [c]IWI – prepared by incipient wetness impregnation.

2.4. Characterization of parent zeolites and Ag-based ZSM-5 adsorbents

Powder X-ray diffraction patterns were recorded on a D8 Advance diffractometer (Bruker) using Cu Kα radiation filtered by Ni and 1D LynxEye detector. Thermogravimetric data (TG-

DSC) were obtained using a Setsys Evo15 Setaram equipment, under air at a heating rate of 10°C min^{-1}. The amount of Ag metal introduced by either IE or IWI was determined through bulk chemical analysis using atomic absorption spectroscopy (AAS) and inductively coupled plasma-optical emission spectroscopy (ICP-OES) techniques. Diffuse reflectance spectroscopy (DRS) UV-Visible spectra were recorded with the assistance of Praying Mantis diffuse reflectance accessory, coupled to a Cary 5000 spectrophotometer (Varian). Ag-based adsorbents were also characterized by H_2-TPR experiments, using an automated Autochem II 2920 apparatus (Micromeritics). The silver-containing zeolites were first pre-treated under Argon (25 $ml.min^{-1}$) at 250 ºC for 1 h and then cooled down to RT. Afterwards, the samples were heated from RT up to 900 ºC (10 $ºC.min^{-1}$) under a 5% H_2/Ar mixture (30 $ml.min^{-1}$). H_2 consumption was monitored by a thermal conductivity (TCD) detector. A cold trap was used to eliminate any water formed during the reduction processes.

2.5. Dynamic adsorption (breakthrough curves) experiments

To assess the performance of the Ag-based zeolite adsorbents, ethylene breakthrough curves (BC) experiments were performed using a fixed-bed adsorption column with a 5 mm internal diameter. Gas analyses were carried out using a gas chromatography GC-2010 Plus (Shimadzu) apparatus, equipped with a flame ionization detector (FID). In a typical experimental run, 100 mg of adsorbent were mixed with 200 mg of silicon carbide (SiC) and loaded into the adsorption column. First, the sample was heated at 250 ºC (10 ºC/min) for 25 min under nitrogen (50 $ml.min^{-1}$). The sample was cooled down to 0 ºC using a thermostatic bath (Haake GH). Breakthrough adsorption experiments were performed under both wet and dry conditions. For both conditions, a gas mixture comprising 500 ppm of C_2H_4 in He, diluted with N_2 to reach a final concentration of 50 ppm, was used. For experiments under wet conditions, a relative humidity of 80% was achieved by passing a N_2 flow through a water bubbling system at 0 ºC. All the experiments were terminated when the ethylene concentration in the effluent reached the concentration of the feed (C/C_0=1). Figure 1 illustrates the experimental setup scheme (wet conditions) used for breakthrough curves adsorption experiments. The breakthrough time and total ethylene adsorption capacity were determined from the breakthrough curves experiments. For some samples, BC experiments

were repeated to ensure reproducibility and to generate additional experimental data for the ANOVA statistical analysis.

FIGURE 1

3. Results and discussion

3.1. Evaluation of the maximum ethylene adsorption capacity

To evaluate the maximum ethylene adsorption capacity of the different Ag-based ZSM-5 adsorbents, ethylene breakthrough curves experiments were done. Two opposite situations were examined, namely wet and dry conditions. In both cases, a low C_2H_4 concentration (50 ppm) and adsorption temperature (0 ºC) were used to replicate conditions close to those found in cold storage chambers. The following sections summarize the different results obtained.

3.1.1. Breakthrough curves under dry conditions

Figure 2 displays the BC results obtained for the different adsorbents, in the absence of water. All the adsorbents exhibit a characteristic "S-shaped" profile, with an adsorption breakthrough curve increasing up to $C/C_0 = 1.0$ and then remaining nearly constant. From these BC results, both break point times and maximum ethylene adsorption capacities were determined and are presented in Table 2. For ZSM-5 adsorbents with a Si/Al ratio of 40, the break point time is relatively short but increases with the increase of Ag amount in the adsorbent, being 3.9Ag-Na(40) sample the one presenting the highest Ag amount along the series. For the ZSM-5(15) series, a longer break point time is observed, when compared with the previous series, but again, it increases with the increase of Ag content. Indeed, in a first approximation, it appears that the ethylene maximum capacity (directly related to the break point time) is correlated with the amount of silver in the respective adsorbent. In other words, the higher the Ag amount, the greater the C_2H_4 max. capacity (see Table 2).

FIGURE 2

3.1.2. Breakthrough curves under wet conditions

Under wet conditions, the various BC profiles obtained significantly differ from those observed in the absence of water (see Figure 3). For all the adsorbents, the breakthrough curves no longer exhibit the usual "S-shaped" profile. Instead, the adsorption curves rise to $C/C_0 > 1$ and then decrease back to 1. These profiles are typically observed when competitive adsorption occurs, as ethylene and H_2O molecules can compete for the same adsorption sites. In both series (Si/Al = 15 and 40), this competitive adsorption phenomenon diminishes with the increasing amount of Ag in the final material and might be related with the fact that the number of compensating cations (either H^+ or Na^+) decreases as the Ag content increases. Furthermore, as already observed for the experiments performed under dry conditions, breakthrough curves for the ZSM-5(15) series are shifted to the right (increase in the break point time) when compared with the ZSM-5(40) series. This indicates that adsorbents with a larger amount of Ag (i.e., Ag-ZSM-5(15) samples), present a higher C_2H_4 adsorption capacity (see Table 2).

FIGURE 3

Table 2. Break point and maximum ethylene capacity obtained from the breakthrough curves experiments.

Sample	Si/Al	Ag (wt. %)	dry conditions		wet conditions	
			Break point[a]	Max. ethylene capacity[b]	Break point[a]	Max. ethylene capacity[b]
H(15)	15	-	7	14*	12	8
Na(15)	15	-	6	21*	-	-
0.7Ag-H(15)	15	0.7	83/83	106/111	53	8*
3.1Ag-H(15)	15	3.1	164	195	66	49
4.3Ag-Na(15)	15	4.3	194	239	67	58
4.6Ag-H(15)	15	4.6	361	451*	64	79
6.1Ag-Na(15)	15	6.1	461	517*	72	105
H(40)	40	-	1	9*	-	-
Na(40)	40	-	-	-	-	-
0.5Ag-H(40)	40	0.5	44/41/41	62/55/60	32	7
1.9Ag-H(40)	40	1.9	107/95/87	124/126/117	39	23
3.2Ag-Na(40)	40	3.2	141	161*	70	97
2.8Ag-H(40)	40	2.8	149	193	43/47/50/51	56/56/56/60
3.9Ag-Na(40)	40	3.9	243	268	65/66	87/94
6.1Ag-H(40)	40	6.1	241	270*	87	125

[a] min; [b] $\mu mol.g^{-1}$; * discarded data to build the refined model; BC experimental conditions: 50 ppm ethylene, 80% RH (wet conditions), gas feed 25 $ml.min^{-1}$, bath temperature 0 ºC.

3.2. Statistical analysis of the maximum ethylene capacity results

Different samples, representing different characteristics of the solid sorbents, were evaluated to determine the ethylene adsorption capacity under both wet and dry conditions, as outlined in Table 2. In some cases, multiple BC results were obtained for a single sample to enhance the input data for the statistical analysis. The observed aggregate variability found within the ethylene adsorption data was separated into two parts: systematic factors and random factors, using Analysis of Variance (ANOVA) [23]. ANOVA was used to distinguish the impact of independent variables on the dependent variables (i.e., ethylene adsorption capacity) and build an adequate regression model. This model aids in understanding the relationship between the ethylene adsorption capacity and the four independent variables representing distinct characteristics of the solids used as adsorbents. The first independent variable (A) was the zeolite Si/Al ratio. The second (B) was the cation exchange rate, defined as 0 for the zeolite in its protonic form (H^+) and 1 when the zeolite is completely exchanged with sodium (Na^+). The third (C) was the amount of added silver expressed in wt.%. The fourth variable (D) was the relative humidity (RH) used in the adsorption test experiments, which was 0% for the "dry" tests and 80% for the "wet" ones.

To perform the ANOVA, some diagnostics tests were performed. These included the normal probability plot to analyze whether the residuals follow a normal distribution, the residuals versus predicted plot to test the assumption of constant variance, and both the residuals versus run and the predicted versus actual response values plots to detect any values or group of values that were not easily predicted by the model (see Figure S1). Based on the diagnostic test, a total of eight samples were discarded as indicated in Table 2 by the asterisk (*). Subsequently, ANOVA was performed to obtain the refined regression model. The Model F-value obtained was 134.37, indicating that the model is statistically significant (p-value <0.0001), i.e., there is only a 0.01% chance that such a large F-value could occur due to random variation. The refined regression model is presented in Equation 1. It can be used to obtain the predicted values of ethylene capacity adsorption at any point within the experimental region.

$$C_2H_4\ capacity = 88.61 - 1.35A - 24.23B + 35.21C - 0.63D + 1.20AB + 0.41AC - 0.35CD \qquad (Eq.1)$$

The ANOVA was used to test both the overall model as well as the individual terms. Figure S1 presents the diagnostic plots used to check the assumptions of the model [24], generated with Design Expert, version 13 from Stat-Ease, Inc. The normal probability plot of the residuals indicates that the residuals follow an approximately normal distribution without the need of any transformation in the response. The residuals follow approximately a straight line with no definite patterns that would require a transformation in the response variable. The plot of residuals versus ascending predicted response values exhibits a random scatter, confirming the validation of the assumption of constant variance. Also, the plot of the residuals versus the experimental run order shows a random scatter with no evidence for any trend that could indicate the presence of a time-related variable in the background. Comparisons between the values predicted by the model and the experimental response values reveal that the model effectively describes the ethylene adsorption capacity. The predicted values closely align with experimental values, indicating an acceptable fitting. Model graphs for statistically significant interactions AB, AC and CD, are presented in Figures 4, 5 and 6.

The AB interaction is significant, with an F value of 5.89 with a p-value of 0.0253. The ethylene adsorption capacity consistently increases when the Si/Al ratio (variable A) is higher (i.e., 40) and the Na exchange rate (variable B) is at the higher level (corresponding to the Na form) (Figure 4). As we can see from the plots, it is important to have higher amounts of silver (i.e., see b) and d)). Additionally, when comparing dry versus wet conditions, it becomes evident that presence of water strongly reduces ethylene adsorption capacity.

FIGURE 4

The AC interaction is significant with an F value of 10.91 and a P-value of 0.0037 meaning that the interaction is not a result of chance. The response value constantly increases when the Si/Al ratio is higher, and the amount of silver is higher (Figure 5). Once more, the detrimental effect of humidity is noticeable, leading to a reduction in ethylene adsorption capacity. Conversely, the beneficial effect of the zeolite in its Na form is evident, contributing to the increase of the dependent variable, i.e., ethylene adsorption capacity.

FIGURE 5

The CD interaction is highly significant with a huge F value of 93.23 corresponding to a very low P-value (<0.0001). This suggests a robust interaction between the amount of silver and

the relative humidity amount (i.e., wet versus dry conditions). The higher response is obtained with a greater amount of silver and under dry conditions as illustrated in Figure 6. The two plots at the top correspond to the protonic form of the zeolite (i.e., variable B=0) while the other two at the bottom represent the sodium form. So, the Na form corresponds to higher response values when the Si/Al ratio is higher (40), but when the Si/Al ratio is 15, the protonic form performs slightly better than the Na form.

FIGURE 6

The fitted regression model is helpful to predict the working conditions within the studied independent variables space, offering predictions and interval estimates. Confirmation allows comparing the prediction interval of the regression model to follow up confirmation samples. If the samples fall within the prediction interval, the model is considered confirmed [25]. To validate the regression model, two new samples were prepared from a ZSM-5 zeolite with a Si/Al ratio of 25 (see Table S1), in its protonic form and with silver amounts of 2.2 and 3.4 wt.%. These samples were designed to assess the adsorption capacity of ethylene under wet conditions thereby confirming the validity of the model. The results, presented in Table S2, reveal that the maximum ethylene adsorption capacities observed are within the prediction interval (PI) of the model for each individual run.

The fitted regression model for ethylene adsorption capacity values (presented in Table 2) was obtained from a limited set of experimental observations corresponding to the samples prepared, with the exclusion of outliers. The model was validated with two confirmatory experiments. Despite the error, it predicts for 95% confidence level the results obtained, within the range of experimentation.

According to the predicted model, the three main factors, namely Si/Al ratio, Na ion exchange rate and relative humidity, contribute negatively to the model, indicating that the individual effect of these factors would contribute to a higher value of ethylene adsorption capacity when these main factors are set to their lowest levels. On the contrary, the amount of Ag has a positive contribution, indicating that a higher amount of Ag corresponds to an increased adsorption capacity. However, upon analyzing interactions, it becomes apparent that the interactions between the Si/Al ratio and the Na exchange rate (AB) and between the Si/Al ratio and the amount of Ag (AC) have positive contributions to ethylene adsorption capacity. The impact of these interactions is stronger than that of the individual main factors,

suggesting that interactions effects hid the effects of the individual main factors. Therefore, the recommended levels of work for the Si/Al ratio, the Na exchange ratio and the amount of Ag should be selected based on the analysis of the interactions.

3.3. On the nature of the interaction between ethylene and adsorbents active sites

The ethylene adsorption capacity of the different Ag-ZSM-5 adsorbents essentially depends on the amount of silver and the presence of water, as revealed by the statistical analysis above. However, other parameters such as the Si/Al ratio and the nature of the compensating cation, also influence the final ethylene adsorption capacity values. To better understand the effect of each parameter and, especially, the beneficial role of Ag in the adsorption performance of ethylene, samples were characterized by X-ray diffraction, UV-Vis DRS spectroscopy and H_2-TPR measurements. It is important to note that, for each ZSM-5 support, the silver amount corresponding to a hypothetical ion exchange rate of 100% is 10.1 and 4.2 wt.% for parent ZSM-5(15) and ZSM-5(40) zeolites, respectively. In fact, the Si/Al ratio of each adsorbent series directly determines the amount of Ag introduced. For the ZSM-5(40) series, the range of Ag content is rather low (0.5-3.9 wt.%) while the range is higher for the ZSM-5(15) series (0.7-6.1 wt.%). In particular, to achieve a relatively high Ag content for ZSM-5(40) material, the incipient wetness impregnation method had to be used (6.1Ag-H(40) sample). The following section summarizes the main results obtained concerning the characterization of the Ag-based adsorbents.

3.3.1. XRD structural analysis of Ag-based ZSM-5 adsorbents

The diffraction patterns obtained for the different samples are presented in Figure S2 (Si/Al series of 15 and 40, respectively). The corresponding raw zeolite materials are also presented, for better comparison. In Figure S2, one can see that all the diffraction patterns are similar to their respective parent zeolites and correspond to ZSM-5 material with a MFI structure (COD-1540301 file number). Also, the intensity of the diffraction peaks slightly decreases in all cases with the increase of the Ag amount in the respective sample, likely due to the strong X-rays absorption by silver species. Zhang and coworkers also verified the same behavior for their silver exchanged Y zeolite material [26]. Nonetheless, as the amount of Ag can be non-negligible for some samples (0.5-6 wt.%), a dilution effect could also contribute to explain

this decrease of intensity to some extent. Moreover, no peaks evidencing the presence of either Ag or Ag_2O phases are observed in all the PXRD patterns, except for sample 6.1Ag-H(40). In this case (Figure S3), extra peaks from hexagonal Ag_2O [27] and cubic Ag^0 (with the former presenting peaks much more intense than the latter) can be observed, together with the peaks of the zeolite support. This result can be explained by the fact that, for this sample, the amount of Ag exceeds the theoretical value corresponding to an ion exchange of 100% (6.1 against 4.2 wt.%, vide supra), meaning that an over exchange has occurred and, logically, species other than monovalent Ag^+ at the exchange positions are observed.

3.3.2. Silver species in Ag-based adsorbents: UV-Vis DRS study

Figure 7 presents the DRS spectra (reflectance mode) obtained for the various Ag-based adsorbents. At first glance, one can see that almost all the spectra are dominated by two intense bands at about 210 and 225 nm, respectively. These bands maxima are in the spectral region generally attributed to the $4d^{10}$-$4d^9 5s^1$ electronic transition of isolated Ag^+ cations [14,28,29]. This means that, regardless of the Si/Al ratio and the Ag amount, these species are well stabilized in the ZSM-5 structure, prevailing as the main species in the final materials. This observation agrees well with the literature, where Ag^+ has been demonstrated to readily and completely exchange into zeolites from aqueous solution [30]. In contrast, the 6.1Ag-H(40) sample is the only exception, as its spectrum is somewhat different: the two bands from isolated Ag^+ species are still observed; however, the spectrum is now dominated by a large band with a maximum at ca. 410 nm.

FIGURE 7

According to the literature, this maximum band appears in the region where signals for Ag_2O or Ag^0 phases can be observed [31]. As indicated by the structural results, it seems that the Ag_2O phase detected by XRD diffraction is present in a larger amount than the Ag^0 phase. We can logically argue that the UV-Vis peak at 410 nm essentially comes from silver oxide species. We will see, later, that the exact nature of these Ag species can be specified in more detail. Finally, all the adsorbents, with the exception of 6.1Ag-H(40) one, exhibit additional bands at 320 and 450 nm, together with the characteristic bands of isolated Ag^+. These bands can be attributed to $Ag_n^{\delta+}$, Ag_m and Ag^0, respectively [31] and their intensity increases with

the amount of Ag. However, the amount of these Ag species in the different adsorbents might be relatively low, as the corresponding bands are only visible when DRS spectra are plotted as reflectance signal versus wavelength. To gain insights into the nature and reducibility of the cationic Ag species present in the adsorbent materials, H_2-TPR experiments were performed.

3.3.3. Amount and reducibility of silver species by H_2-TPR experiments

FIGURE 8

The H_2-TPR profiles obtained for each silver-based adsorbent are presented in Figure 8. Several peaks are observed over the entire reduction temperature range (30-800 ºC), but they can be separated into two different H_2 consumption zones: one at low temperature (LT, 50-250 ºC, narrow range) and the other at a higher temperature (HT, 300-700 ºC, large range). According to the literature, monovalent Ag^+ species might not reduce directly to Ag^0 but instead undergo a two-step reduction, one at LT and the second at a higher temperature, being $Ag_n^{\delta+}$ the intermediate species [28,29,31–33] (see Equation 2). Determining the exact nature of these intermediates is not easy, as it depends on several parameters like the Ag amount, the zeolite structure, the Si/Al ratio, or the reducing treatment conditions. Nevertheless, the following authors identified possible $Ag_n^{\delta+}$ candidates for Ag-zeolite systems similar to our: Ag_4^{2+} in ZSM-5-based materials [28] and Ag_4^{2+}/Ag_3^+ in CHA-based ones [34].

$$Ag^+ \xrightarrow{LT} Ag_n^{\delta+} \xrightarrow{HT} Ag^0 \qquad \text{Eq. 2}$$

Interestingly, the results from Shibata *et al.* [28] were obtained with similar starting materials (ZSM-5, Si/Al=15 or 22), Ag loadings (1.7-3.5 wt.%) and samples preparation conditions (ion exchange) as applied in this work. The H_2/Ag molar ratio they obtained (about 0.25) for the two reduction peaks supports the hypothesis that Ag_4^{2+} species are the main intermediates during Ag^+ reduction process. In our case, a similar H_2/Ag ratio (0.25) was observed for the first reduction peak, but not for the second. This second peak occurs over a larger temperature range and its area is always equal or higher than that of the first reduction peak, except for the 6.1Ag-H(40) material, where the first reduction peak is the most intense. For Na^+ samples, the

second reduction peak occurs at a relatively lower temperature while, for H^+ samples, the reduction temperature is much higher. Berndt *et al.* investigated the influence of Brönsted acid sites on the redox properties of silver-based mordenite materials [35]. They concluded that Ag^+ reduction process was strongly influenced by Brönsted acid sites concentration as well as by the degree of Ag^+ exchange. A shift of the reduction peak to higher temperatures was observed in the presence of H^+ (instead of Na^+) in the Ag-exchanged samples. Our results match well the ones from Berndt *et al.* [36].

3.4. Discussion on the relationship between Ag species and ethylene molecules

In order to understand better the capacity of the different Ag-base zeolites in adsorbing selectively ethylene and the specific roles played by the different Ag species, an effort was made to correlate the maximum C_2H_4 capacity with the amount of both Ag and Ag^+ species. The data summarizing hydrogen consumption, derived from H_2-TPR experiments, are presented in Table 3. For each sample, the table includes theoretical and experimental hydrogen consumptions, along with the contribution of each reduction peak, the one at low temperature and the other at higher temperature. Table 3 also provides information on ethylene adsorption capacity obtained under both dry and wet conditions.

Table 3. Maximum ethylene capacity and amount of Ag, Ag^+ and $Ag_n^{\delta+}$ species for the different adsorbents under study

Sample	Ag (wt. %)	Theo H_2[a]	Exp. H_2[a]	1st peak [a(b)]	2nd peak [a]	max. C_2H_4 capacity[b]	
						dry	wet
0.7Ag-H(15)	0.7	0.78	0.63	0.16 (26)	0.47	108 [c]	8
3.1Ag-H(15)	3.1	3.51	3.27	0.94 (154)	2.33	195	49
4.3Ag-Na(15)	4.3	4.87	3.12	1.24 (203)	1.88	239	58
4.6Ag-H(15)	4.6	5.21	5.14	1.99 (325)	3.16	451	79
6.1Ag-Na(15)	6.1	6.91	5.27	2.71 (443)	2.56	517	105
0.5Ag-H(40)	0.5	0.59	0.49	0.12 (20)	0.37	59 [c]	7
1.9Ag-H(40)	1.9	2.15	1.71	0.71 (116)	1.00	122 [c]	23
3.2Ag-Na(40)	3.2	3.63	2.57	1.14 (187)	1.43	161	97
2.8Ag-H(40)	2.8	3.17	2.56	1.15 (188)	1.41	193	57 [c]
3.9Ag-Na(40)	3.9	4.42	3.07	1.44 (236)	1.63	268	91[c]
6.1Ag-H(40)	6.1	6.91	3.78	2.85 (466)	0.93	270	125

[a] $ml.g^{-1}$; [b] $\mu mol.g^{-1}$; [c] average value (see Table 1).

Figure 9 displays the correlation between the experimental hydrogen consumption and the theoretical one. The latter was calculated from the amount of silver in each sample, assuming all the Ag present was fully oxidized (Ag^+). Interestingly, for low Ag content and for both series (Si/Al= 15 and 40), the experimental H_2 consumption fairly follows the theoretical values, meaning that silver is primarily introduced as Ag^+ exchanged species. However, for higher silver content (> 3 wt.%), the experimental consumption deviates downward, with a more pronounced deviation observed for the Si/Al=40 series. This observation is well consistent with the fact that: a) Ag can be easily introduced within the zeolites as Ag^+ exchanged species [30]; b) for exchange rate values close to 100 % or higher, Ag species other than Ag^+ begin to appear. This is especially the case for 6.1Ag-H(40) sample. As shown earlier, this sample is the only one where over exchange occurred. As this sample presents an intense UV-Vis signal at 410 nm and a highly pronounced reduction peak at low temperature (LT), one can assume that Ag_2O species coexist with Ag^+ species in this sample. For all the other samples, for both 15 and 40 series, the amount of Ag is below 10.1 (the theoretical value for 100% Ag exchange for Si/Al=15) or 4.2 (Si/Al=40). In this case, the main Ag species are isolated Ag^+, although some partially oxidized Ag clusters may be present, as observed in the respective DRS UV-Vis spectra.

FIGURE 9

Figure 10 shows the ethylene adsorption capacity as a function of the amount of Ag^+ concentration for both series and under both dry and wet conditions. The Ag^+ concentration is calculated from the first reduction peak, assuming that intermediates Ag species in *equation 1* are partially charged Ag_4^{2+} clusters, as stated by Shibata *et al.* [28]. Under dry conditions (Figure 10, A), a reasonable linear correlation between C_2H_4 adsorption and Ag^+ concentration is observed for both series, with a C_2H_4/Ag^+ ratio of about 1.10. This agrees with the finding of Cisneros *et al.* [17] who also reported an increase of ethylene adsorption with the amount of charged Ag species in the zeolite adsorbent. This one-to-one C_2H_4/Ag^+ ratio is consistent with the results of Texter and coworkers, who performed ethylene adsorption experiments followed by UV-Vis DRS spectroscopy and thermogravimetric measurements [37]. The exception is the 6.1Ag-H(40) sample, where a substantial amount of silver exists as Ag_2O species, leading to an overestimated Ag^+ concentration calculated from the first reduction peak. Consequently, the data point coordinates for the 6.1Ag-H(40) sample may shift and align with the linear regression (as indicated by the arrow in Figure 10, A).

Under wet conditions, the situation is quite different (Figure 10, B). Two different regression lines can be obtained, one for each series. For sample 6.1Ag-H(40) data point coordinates may shift to the left and align with the Si/Al=40 series regression line. In presence of water, the C_2H_4/Ag^+ ratio (linear slope) decreases to about 0.42 for the 40 series and 0.22 for 15 series, indicating competitive adsorption between ethylene and water and a subsequent reduction in ethylene capacity for all the adsorbents. Interestingly, the ethylene/Ag^+ ratios observed, either under dry or wet conditions, are well in line with the results from Kang *et al.* [21] who studied an Ag-based BEA zeolite system for hydrocarbons cold-start trapping. The more hydrophobic samples (40 series) appear to exhibit better performance under wet conditions.

FIGURE 10

4. Conclusions

In this study, a series of Ag-based ZSM-5 materials, with different Ag contents (0-6 wt.%), two Si/Al ratios (15 and 40) and two compensating cations (Na^+ and H^+), was prepared. All the adsorbents were tested in ethylene adsorption tests using breakthrough curves experiments under both dry and wet conditions, with an initial low ethylene concentration (50 ppm) to simulate the atmosphere of industrial cold storage chambers. The results demonstrated the high efficiency of the samples in ethylene adsorption, reaching a maximum ethylene capacity of approximately 500 $\mu mol.g^{-1}$ under dry conditions. In the presence of water, a competitive adsorption between ethylene and H_2O was observed, leading to a decrease in the maximum ethylene capacities to 100-125 $\mu mol.g^{-1}$. Isolated Ag^+ species located at the exchange positions were identified as the main responsible for the excellent adsorbents' performance as these species can interact strongly with ethylene through π interaction. Under dry conditions, a fairly one-to-one relationship, between cationic Ag^+ species and ethylene, was observed. However, in the presence of water, the ethylene/Ag^+ ratio significantly decreased. Notably, adsorbents with a higher hydrophobic character (higher Si/Al ratio) demonstrate better resistance in the presence of water.

The statistical analysis of variance ANOVA performed on this system revealed the existence of strong interactions among the different parameters studied, namely the Si/Al ratio, Na exchange ratio and Ag amount. Therefore, the operating levels of work recommended for these parameters should be determined based on a thorough analysis of these interactions.

Acknowledgements

The authors thank FCT for providing funding through projects (Nano4fresh-PRIMA/0015/2019 (http://doi.org/10.54499/PRIMA/0015/2019)) (UIDB/00100/2020 (https://doi.org/10.54499/UIDB/00100/2020)) and UIDP/00100/2020 (https://doi.org/10.54499/UIDP/00100/2020)-CQE and (LA/P/0056/2020 (https://doi.org/10.54499/LA/P/0056/2020))-IMS. A.F. thanks Instituto Superior Técnico for the Scientific Employment contract under law DL 57/2016. R. Ferreira extends thanks FCT for the PhD grant (2022.12593.BD).

Authors contribution

Conceptualization: A.F., I.M.J., J.M.S., F.R.; **Investigation**: R.F., H.L., A.F.; **Formal analysis,** I.M.J., J.M.S.**; writing—original draft preparation**, R.F.; **writing—review and editing**, A.F., J.P.L., I.M.J., J.M.S., F.R.; **Visualization:** A.F., I.M.J., J.M.S.; **supervision**; A.F., F.R.; **project administration**, F.R.; **funding acquisition**, F.R. All authors have read and agreed to the published version of the manuscript.

References

[1] N. Keller, M.-N. Ducamp, D. Robert, V. Keller, Ethylene Removal and Fresh Product Storage: A Challenge at the Frontiers of Chemistry. Toward an Approach by Photocatalytic Oxidation, Chem. Rev. 113 (2013) 5029–5070. https://doi.org/10.1021/cr900398v.

[2] N. Pathak, P. Mahajan, Ethylene Removal From Fresh Produce Storage: Current Methods and Emerging Technologies, in: Reference Module in Food Science, Elsevier, 2017. https://doi.org/10.1016/B978-0-08-100596-5.22330-5.

[3] S. Bodbodak, M. Moshfeghifar, 2 - Advances in controlled atmosphere storage of fruits and vegetables, in: M.W.B.T.-E.-F.T. for P.P.Q. Siddiqui (Ed.), Eco-Friendly Technology for Postharvest Produce Quality, Academic Press, 2016: pp. 39–76. https://doi.org/10.1016/B978-0-12-804313-4.00002-5.

[4] Q. Zhang, S. Gao, J. Yu, Metal Sites in Zeolites: Synthesis, Characterization, and Catalysis, Chem. Rev. 123 (2023) 6039–6106. https://doi.org/10.1021/acs.chemrev.2c00315.

[5] D. Saha, M.-B. Kim, A.J. Robinson, R. Babarao, P.K. Thallapally, Elucidating the mechanisms of Paraffin-Olefin separations using nanoporous adsorbents: An overview, IScience 24 (2021) 103042. https://doi.org/10.1016/j.isci.2021.103042.

[6] A.W.J. Smith, S. Poulston, L. Rowsell, L.A. Terry, J.A. Anderson, A new palladium-based ethylene scavenger to control ethylene-induced ripening of climacteric fruit, Platin. Met. Rev. 53-3 (2009) 112-122. https://doi.org/10.1595/147106709X462742.

[7] J. Tzeng, C. Weng, J. Huang, C. Shiesh, Y. Lin, Y. Lin, Application of palladium-modified zeolite for prolonging post-harvest shelf life of banana, J. Sci. Food Agric. 99 (2019) 3467–3474. https://doi.org/10.1002/jsfa.9565.

[8] D. Vargas-Hernández, M.A. Pérez-Cruz, R. Hernández-Huesca, Selective adsorption of ethylene over ethane on natural mordenite and on K^+-exchanged mordenite, Adsorption 21 (2015) 153–163. https://doi.org/10.1007/s10450-015-9658-8.

[9] J. de Bruijn, A. Gómez, C. Loyola, P. Melín, V. Solar, N. Abreu, F. Azzolina-Jury, H. Valdés, Use of a Copper- and Zinc-Modified Natural Zeolite to Improve Ethylene Removal and Postharvest Quality of Tomato Fruit, Crystals 10 (2020) 471-477. https://doi.org/10.3390/cryst10060471.

[10] A. Coloma, F.J. Rodríguez, J.E. Bruna, A. Guarda, M.J. Galotto, Development of an active film with natural zeolite as ethylene scavenger, J. Chil. Chem. Soc. (2014) 2409-2414. https://doi.org/10.4067/S0717-97072014000200003.

[11] G. Aguilar-Armenta, Á. Romero-Pérez, Adsorption of C_2H_4, C_2H_6 and CO_2 on Cation-exchanged Clinoptilolite, Adsorpt. Sci. Technol. 27 (2009) 523–536. https://doi.org/10.1260/0263-6174.27.5.523.

[12] B. Erdoğan, M. Sakızcı, E. Yörükoğulları, Characterization and ethylene adsorption of natural and modified clinoptilolites, Appl. Surf. Sci. 254 (2008) 2450–2457. https://doi.org/10.1016/j.apsusc.2007.09.058.

[13] J.D. Monzón, A.M. Pereyra, M.R. Gonzalez, M.S. Legnoverde, M.S. Moreno, N. Gargiulo, A. Peluso, P. Aprea, D. Caputo, E.I. Basaldella, Ethylene adsorption onto thermally treated AgA-Zeolite, Appl. Surf. Sci. 542 (2021) 148748. https://doi.org/10.1016/j.apsusc.2020.148748.

[14] J.G. Min, K.C. Kemp, S.B. Hong, Silver ZK-5 zeolites for selective ethylene/ethane separation, Sep. Purif. Technol. 250 (2020) 117146. https://doi.org/10.1016/j.seppur.2020.117146.

[15] Y.S. Mok, S.-G. Kim, D. Ba Nguyen, Q.H. Trinh, H.W. Lee, S.B. Kim, Plasma-catalytic oxidation of ethylene over zeolite-supported catalysts to improve the storage stability of agricultural products, Catal. Today 337 (2019) 208–215. https://doi.org/10.1016/j.cattod.2019.02.059.

[16] H. Abdi, H. Maghsoudi, V. Akhoundi, Adsorption properties of ion-exchanged SSZ-13 zeolite for ethylene/ethane separation, Fluid Phase Equilib. 546 (2021) 113171. https://doi.org/10.1016/j.fluid.2021.113171.

[17] L. Cisneros, F. Gao, A. Corma, Silver nanocluster in zeolites. ADSORPTION of ETHYLENE traces for fruit preservation, Micropor. Mesopor. Mat. 283 (2019) 25–30. https://doi.org/10.1016/j.micromeso.2019.03.032.

[18] Mohammed Wasim Siddiqui, ed., Eco-Friendly Technology for Postharvest Produce Quality, Academic Press, 2016.

[19] C. Horvatits, J. Lee, E.A. Kyriakidou, E.A. Walker, Characterizing Adsorption Sites on Ag/SSZ-13 Zeolites: Experimental Observations and Bayesian Inference, J. Phys. Chem. C 124 (2020) 19174–19186. https://doi.org/10.1021/acs.jpcc.0c06470.

[20] C. Horvatits, D. Li, M. Dupuis, E.A. Kyriakidou, E.A. Walker, Ethylene and Water Co-Adsorption on Ag/SSZ-13 Zeolites: A Theoretical Study, J. Phys. Chem. C 124 (2020) 7295–7306. https://doi.org/10.1021/acs.jpcc.0c00849.

[21] S.B. Kang, C. Kalamaras, V. Balakotaiah, W. Epling, Hydrocarbon Trapping over Ag-Beta Zeolite for Cold-Start Emission Control, Catal. Letters 147 (2017) 1355–1362. https://doi.org/10.1007/s10562-017-2044-2.

[22] J. Lee, K. Giewont, J. Chen, C.-H. Liu, E.A. Walker, E.A. Kyriakidou, Ag/ZSM-5 traps for C_2H_4 and C_7H_8 adsorption under cold-start conditions, Micropor. Mesopor. Mat. 327 (2021) 111428. https://doi.org/10.1016/j.micromeso.2021.111428.

[23] D.C. Montgomery, Introduction to statistical quality control, 8th ed., John Wiley & Sons, Inc., Hoboken, NJ SE -, 2019.

[24] G. Vining, Technical Advice: Residual Plots to Check Assumptions, Qual. Eng. 23 (2010) 105–110. https://doi.org/10.1080/08982112.2011.535696.

[25] D.C. Montgomery, Design and Analysis of experiments, 10th ed., WILEY-VCH Verlag, 2019.

[26] L. Zhang, T. Wulf, F. Baum, W. Schmidt, T. Heine, M. Hirscher, Chemical Affinity of Ag-Exchanged Zeolites for Efficient Hydrogen Isotope Separation, Inorg. Chem. 61 (2022) 9413–9420. https://doi.org/10.1021/acs.inorgchem.2c00028.

[27] N. Ravi Chandra Raju, K. Jagadeesh Kumar, A. Subrahmanyam, Physical properties of silver oxide thin films by pulsed laser deposition: effect of oxygen pressure during growth, J. Phys. D: Appl. Phys. 42 (2009) 135411. https://doi.org/10.1088/0022-3727/42/13/135411.

[28] J. Shibata, K. Shimizu, Y. Takada, A. Shichi, H. Yoshida, S. Satokawa, A. Satsuma, T. Hattori, Structure of active Ag clusters in Ag zeolites for SCR of NO by propane in the presence of hydrogen, J. Catal. 227 (2004) 367–374. https://doi.org/10.1016/j.jcat.2004.08.007.

[29] T. Nanba, S. Masukawa, J. Uchisawa, A. Obuchi, Effect of support materials on Ag catalysts used for acrylonitrile decomposition, J. Catal. 259 (2008) 250–259. https://doi.org/10.1016/j.jcat.2008.08.013.

[30] T. Sun, K. Seff, Silver Clusters and Chemistry in Zeolites, Chem. Rev. 94 (1994) 857–870. https://doi.org/10.1021/cr00028a001.

[31] R. Bartolomeu, R. Bértolo, S. Casale, A. Fernandes, C. Henriques, P. Da Costa, F. Ribeiro, Particular characteristics of silver species on Ag-exchanged LTL zeolite in K and H form, Micropor. Mesopor. Mat. 169 (2013) 137–147. https://doi.org/10.1016/j.micromeso.2012.10.015.

[32] N.D. Hutson, B.A. Reisner, R.T. Yang, B.H. Toby, Silver Ion-Exchanged Zeolites Y, X, and Low-Silica X: Observations of Thermally Induced Cation/Cluster Migration and the Resulting Effects on the Equilibrium Adsorption of Nitrogen, Chem. Mater. 12 (2000) 3020–3031. https://doi.org/10.1021/cm000294n.

[33] Y. Kim, K. Seff, The hexasilver molecule stabilized by coordination to six silver ions. The structure of $(Ag^{+})_6(Ag_6)$. The crystal structure of an ethylene sorption complex of partially decomposed fully Ag^{+} exchanged zeolite A, J. Am. Chem. Soc. 100 (1978) 175–180. https://doi.org/10.1021/ja00469a030.

[34] H.K. Beyer, P.A. Jacobs, Chemical Evidence for Charged Clusters in Silver Zeolites, in: P.A. Jacobs, N.I. Jaeger, P. Jírů, G.B.T.-S. in S.S. and C. Schulz-Ekloff (Eds.), Metal Microstructures in Zeolites, Elsevier, 1982: pp. 95–102. https://doi.org/10.1016/S0167-2991(09)60997-6.

[35] H. Berndt, M. Richter, T. Gerlach, M. Baerns, Influence of Brönsted acidity on the redox properties of silver species in zeolite mordenite, J. Chem. Soc. Faraday T. 94 (1998) 2043–2046. https://doi.org/10.1039/A801524D.

[36] H. Berndt, A. Martin, Y. Zhang, Study on the nature and the redox properties of cobalt species located in CoAPO molecular sieves, Microporous Mater. 6 (1996) 1–12.

[37] J. Texter, T. Gonsiorowski, R. Kellerman, 5s-4d transition of trigonal Ag^+ in zeolite, Phys. Rev. B 23 (1981) 4407–4418. https://doi.org/10.1103/PhysRevB.23.4407.

Figures captions:

Figure 1. Experimental setup used for ethylene adsorption experiments: a) gases mass flowmeters, b) three-way valves, c) thermostatic bath; d) GC-FID gases analyzer.

Figure 2. Breakthrough curves profiles in dry conditions of: (left), ZSM-5(15) adsorbents series and (right), ZSM-5(40) adsorbents series (50 ppm ethylene, gas feed 25 $ml.min^{-1}$, adsorption temperature 0 ºC).

Figure 3. Breakthrough curves profiles in wet conditions of: (left), ZSM-5(15) adsorbents series and (right), ZSM-5(40) adsorbents series (50 ppm ethylene, 80% RH, gas feed 25 $ml.min^{-1}$, bath temperature 0 ºC).

Figure 4. Analysis of the interaction AB in the maximum ethylene adsorption capacity: a) and c) silver amount of 0.5 wt.%; b) and d) silver amount of 6.1 wt.%; a) and b) dry conditions; c) and d) wet conditions (RH of 80%).

Figure 5. Analysis of the interaction AC in the maximum ethylene adsorption capacity: a) and c) H^+ form; b) and d) Na^+ form; a) and b) dry conditions; c) and d) wet conditions (RH of 80%)

Figure 6. Analysis of the interaction CD in the maximum ethylene adsorption capacity: a) and c) Si/Al ratio of 15; b) and d) Si/Al ratio of 40; a) and b) zeolite in the H^+ form; c) and d) zeolite in the Na^+ form.

Figure 7. UV-Vis DRS spectra of samples: A) 0.7Ag-H(15) (a), 3.1Ag-H(15) (b), 4.3Ag-Na(15) (c), 4.6Ag-H(15) (d) and 6.1Ag-Na(15) (e); B) 0.5Ag-H(40) (a), 1.9Ag-H(40) (b), 3.2Ag-Na(40) (c), 2.8Ag-H(40) (d), 3.9Ag-Na(40) (e) and 6.1Ag-H(40).

Figure 8. H_2-TPR profiles of samples: A) 0.7Ag-H(15) (a), 3.1Ag-H(15) (b), 4.3Ag-Na(15) (c), 4.6Ag-H(15) (d) and 6.1Ag-Na(15) (e); B) 0.5Ag-H(40) (a), 1.9Ag-H(40) (b), 3.2Ag-Na(40) (c), 2.8Ag-H(40) (d), 3.9Ag-Na(40) (e) and 6.1Ag-H(40) (f).

Figure 9. Relationship between experimental and theoretical H_2 consumption for Ag-based ZSM-5 adsorbents (dash black line denotes an experimental consumption equal to the theoretical one).

Figure 10. Ethylene maximum adsorption capacity as a function of Ag^+ species content in the adsorbents (determined by H_2-TPR measurements): a) dry conditions and b) wet conditions.

Tables captions:

Table1. Ion exchange conditions for Ag-based adsorbents preparation ($AgNO_3$ aq. solution, RT, under dark, 24 h).

Table2. Break point and maximum ethylene capacity obtained from the breakthrough curves experiments.

Table3. Maximum ethylene capacity and amount of Ag, Ag^+ and $Ag_n^{\delta+}$ species for the different adsorbents under study.

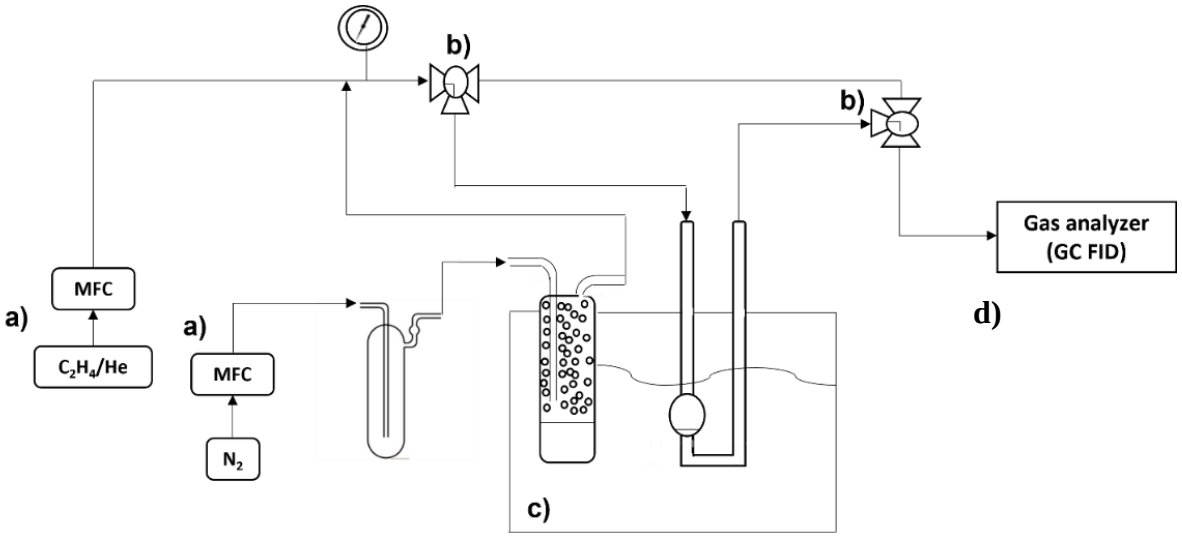
b)
b)
Gas analyzer
(GC FID)
MFC
a)
C_2H_4/He
a)
MFC
N_2
c)
d)

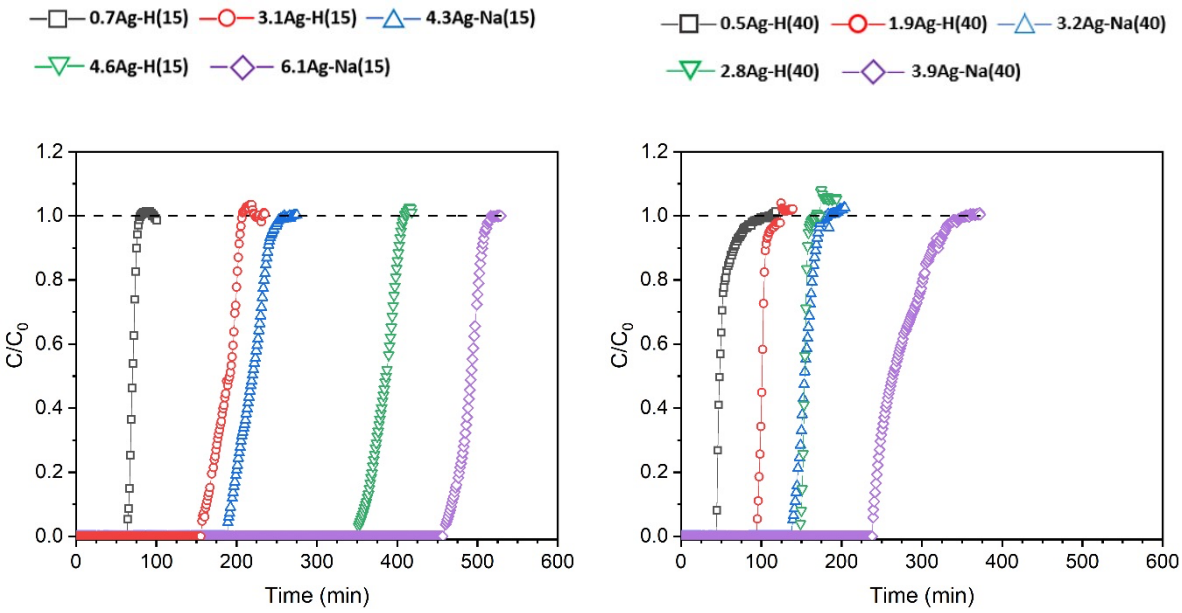
0.7Ag-H(15)
3.1Ag-H(15)
4.3Ag-Na(15)
4.6Ag-H(15)
6.1Ag-Na(15)
0.5Ag-H(40)
1.9Ag-H(40)
3.2Ag-Na(40)
2.8Ag-H(40)
3.9Ag-Na(40)
C/C0
Time (min)
0.0
0.2
0.4
0.6
0.8
1.0
1.2
0
100
200
300
400
500
600

Figure 2

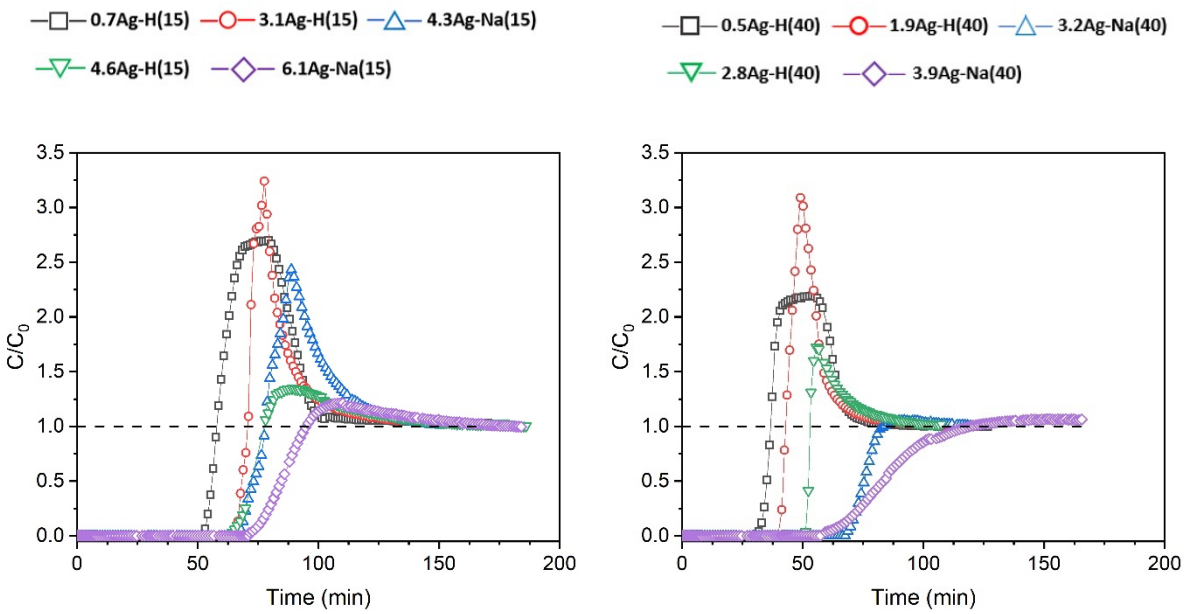
0.7Ag-H(15)
3.1Ag-H(15)
4.3Ag-Na(15)
4.6Ag-H(15)
6.1Ag-Na(15)
0.5Ag-H(40)
1.9Ag-H(40)
3.2Ag-Na(40)
2.8Ag-H(40)
3.9Ag-Na(40)
C/C0
Time (min)
0
50
100
150
200
0.0
0.5
1.0
1.5
2.0
2.5
3.0
3.5

Figure 3

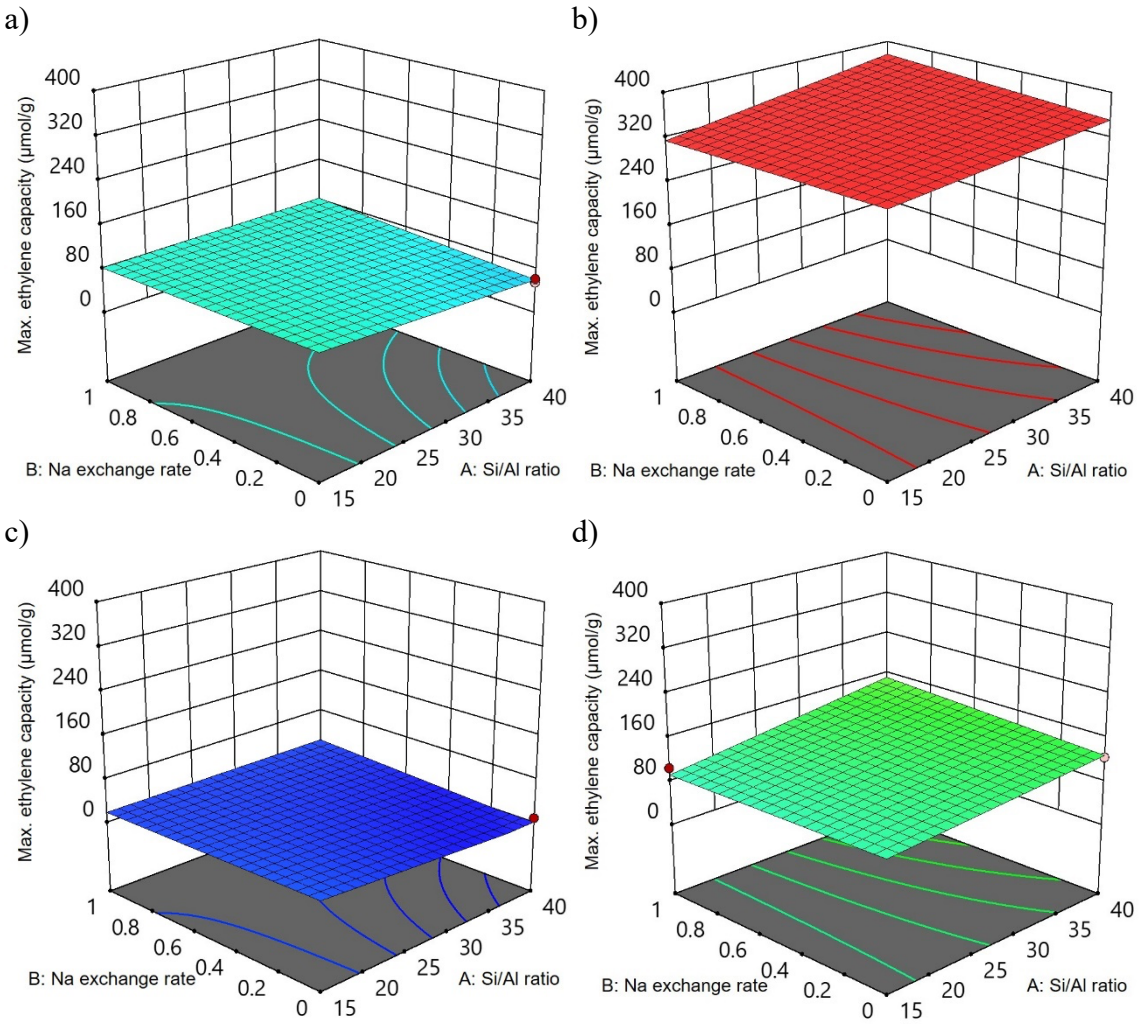
a)
b)
c)
d)
Max. ethylene capacity (µmol/g)
400
320
240
160
80
0
B: Na exchange rate
1
0.8
0.6
0.4
0.2
0
A: Si/Al ratio
15
20
25
30
35
40

Figure 4

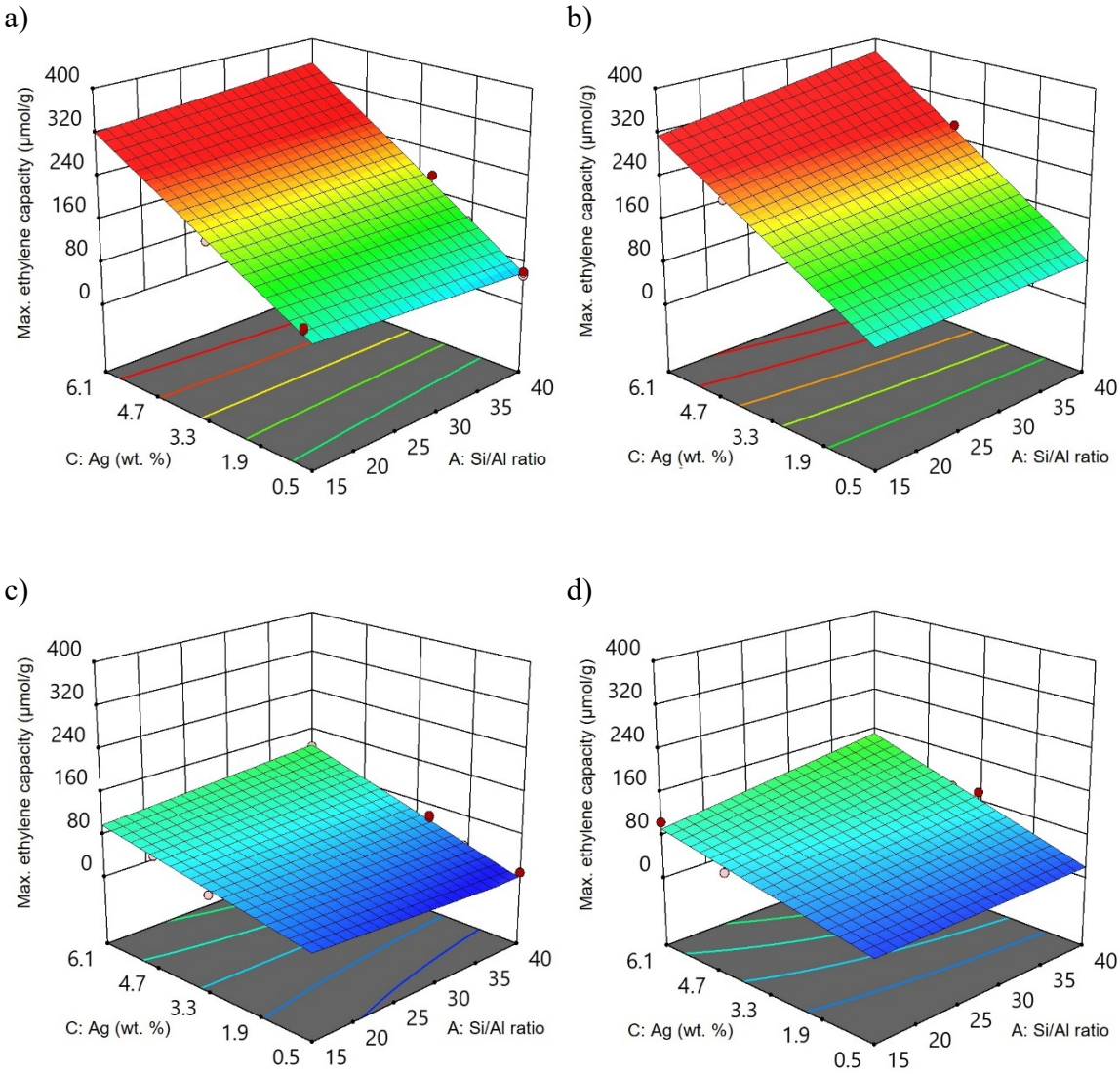
a)
b)
c)
d)
Max. ethylene capacity (µmol/g)
400
320
240
160
80
0
C: Ag (wt. %)
6.1
4.7
3.3
1.9
0.5
A: Si/Al ratio
15
20
25
30
35
40

Figure 5

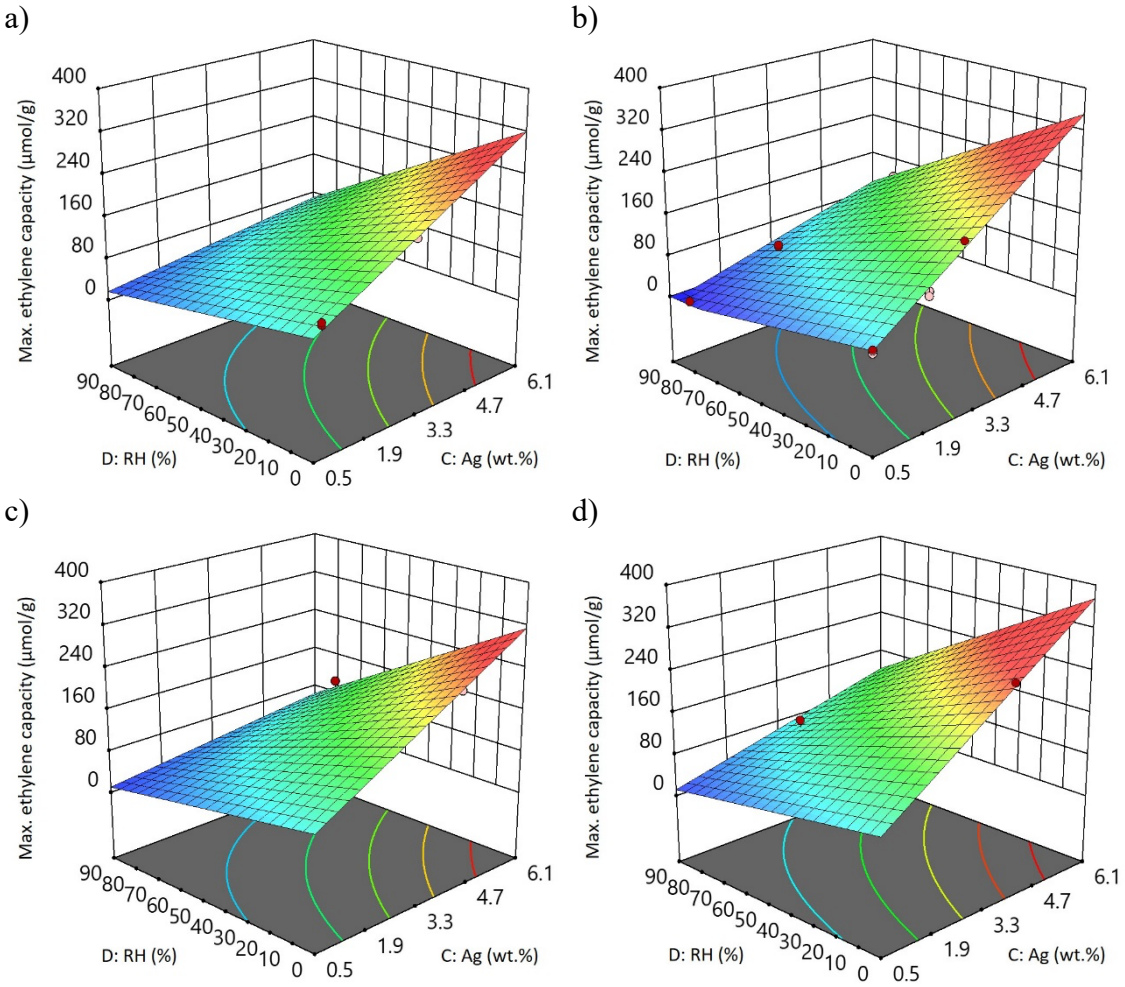
a)
b)
c)
d)
Max. ethylene capacity (µmol/g)
400
320
240
160
80
0
D: RH (%)
90 80 70 60 50 40 30 20 10 0
C: Ag (wt.%)
0.5 1.9 3.3 4.7 6.1

Figure 6

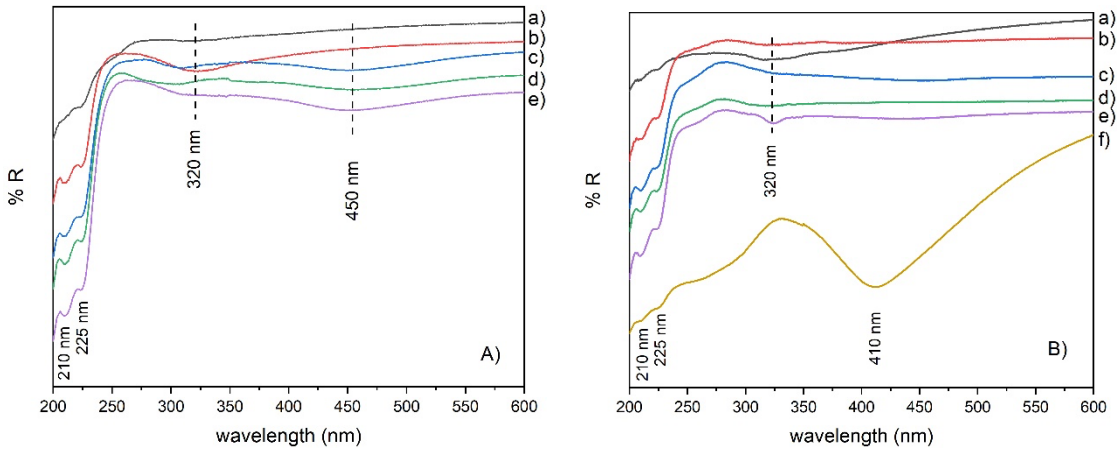

Figure 7

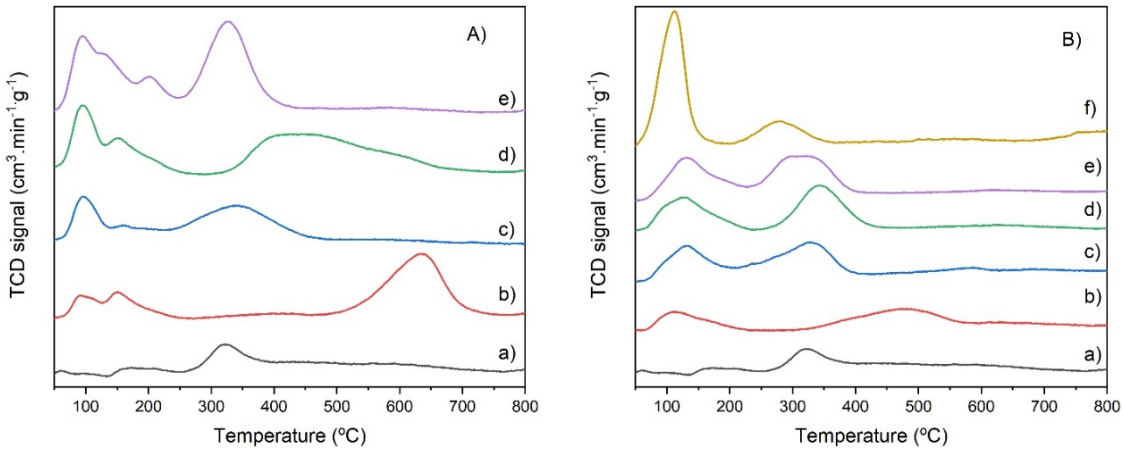
A)
e)
d)
c)
b)
a)
TCD signal (cm3.min-1.g-1)
100
200
300
400
500
600
700
800
Temperature (°C)
B)
f)
e)
d)
c)
b)
a)
TCD signal (cm3.min-1.g-1)
100
200
300
400
500
600
700
800
Temperature (°C)

Figure 8

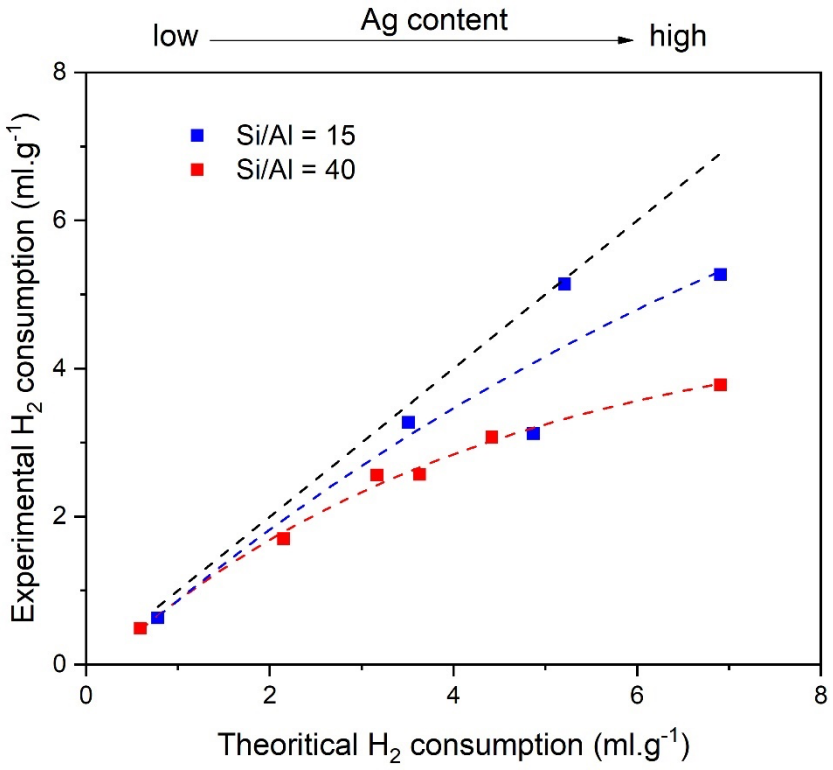
low
Ag content
high
Si/Al = 15
Si/Al = 40
Experimental H2 consumption (ml.g-1)
Theoritical H2 consumption (ml.g-1)
0
2
4
6
8

Figure 9

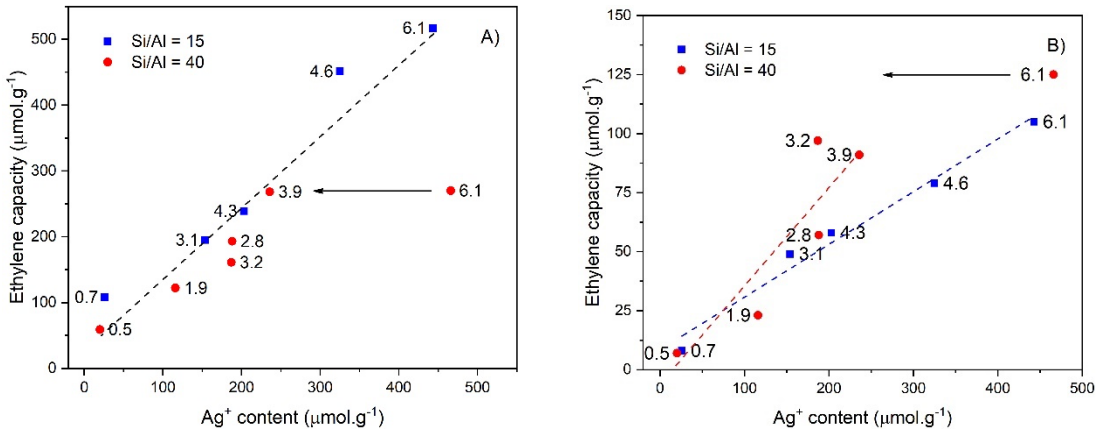
A)
Si/Al = 15
Si/Al = 40
Ethylene capacity (µmol.g-1)
Ag+ content (µmol.g-1)
0
100
200
300
400
500
6.1
4.6
3.9
6.1
4.3
3.1
2.8
3.2
1.9
0.7
0.5
B)
Si/Al = 15
Si/Al = 40
Ethylene capacity (µmol.g-1)
Ag+ content (µmol.g-1)
0
25
50
75
100
125
150
6.1
3.2
3.9
4.6
2.8
4.3
3.1
1.9
0.5
0.7

Figure 10